Interface inductive currents and carrier injection in hybrid perovskite single crystals

Alexander Kovalenko, Jan Pospisil, Jozef Krajcovic, Martin Weiter, Antonio Guerrero, and Germà Garcia-Belmonte

Citation: Appl. Phys. Lett. **111**, 163504 (2017); doi: 10.1063/1.4990788
View online: http://dx.doi.org/10.1063/1.4990788
View Table of Contents: http://aip.scitation.org/toc/apl/111/16
Published by the American Institute of Physics

Interface inductive currents and carrier injection in hybrid perovskite single crystals

Alexander Kovalenko,[1,a)] Jan Pospisil,[1] Jozef Krajcovic,[1] Martin Weiter,[1] Antonio Guerrero,[2] and Germà Garcia-Belmonte[2,a)]
[1]*Materials Research Centre, Faculty of Chemistry, Brno University of Technology, Purkyňova 118, 612 00 Brno, Czech Republic*
[2]*Institute of Advanced Materials (INAM), Universitat Jaume I, 12006 Castelló, Spain*

(Received 18 June 2017; accepted 8 October 2017; published online 19 October 2017)

Interfaces between the absorbing perovskite and transporting layers are gaining attention as the key locus that governs solar cell operation and long term performance. The interplay of ionic and electronic processes, along with the asymmetrical architecture of any solar cell, makes the interpretation of electrical measurements always inconclusive. A strategy to progress in relating electric responses, operating mechanisms, and device architecture relies upon simplifying the probing structure. Macroscopic $CH_3NH_3PbBr_3$ single crystals with symmetrical contacts are tested by means of long-time current transient and impedance spectroscopy. It is observed that interfaces govern carrier injection to (and extraction from) perovskite layers through an inductive (negative capacitance) mechanism with a response time in the range of ∼1–100 s under dark conditions and inert atmosphere. Current transient exhibits a slow recovering after the occurrence of an undershoot, signaling a complex carrier dynamics which involves changes in surface state occupancy. *Published by AIP Publishing*. https://doi.org/10.1063/1.4990788

Interfaces between light absorbing perovskites and contact layers, and as a consequence interface-mediated mechanisms, are recognized to constitute issues of primary concern to progress in our understanding of processes that limit photovoltaic performance. Because of the intrinsic[1–3] (and extrinsic)[4,5] defect transporting character of the perovskite lattice, the interaction between mobile ions and contacting materials has been reported as a source of device instability. It is identified that iodine migrates and reacts with the hole transporting layer (*spiro*-OMeTAD), reducing its conductivity.[6,7] Also, gold or silver from contacts is known to interact with the perovskite layer, opening irreversible degradation pathways.[8,9] Although mobile ions are involved in detrimental solid state reactions, it is also expected that they participate in the alteration of determining electronic processes[10,11] and particularly causing current hysteresis effects.[12–15] For instance, the reversible interaction between iodine and TiO_2 has been proposed to produce charge accumulation at interfaces and capacitive currents.[6] Electrode polarization processes were identified in relation to long time or low frequency features exhibited by perovskite solar cells, both in the dark and under illumination.[16,17] Polarization at contacts, kinetically governed by mobile ions, has been connected to surface carrier recombination and achievable open-circuit voltage.[18,19] A very recent work[20] connects complex dynamics, involving both electronic and ionic charges at outer interfaces, to the occurrence of inductive behaviors observed by impedance spectroscopy. Hence, interfaces between the absorbing perovskite and transporting layers are gaining attention as the key locus that governs the solar cell operation and long term performance.

The analysis of mechanisms at interfaces is certainly elusive. The interplay of ionic and electronic processes, along with the asymmetrical architecture of any solar cell, makes the interpretation of electrical measurements always inconclusive. Photovoltaic devices operate under illumination in such a way that it is usually difficult discerning between light and voltage influences. Furthermore, common perovskite solar cells comprise polycrystalline absorber layers so that the material structure is an extra factor complicating the experimental analysis. A strategy to progress in relating electric responses, operating mechanisms, and device architecture relies upon simplifying the probing structure. This is why single crystal, symmetrical samples are analyzed here.[21–23] By examining long-time current transients and impedance spectroscopy of macroscopic single crystals, it is revealed here that interfaces govern carrier injection to (and extraction from) perovskite layers through an inductive (negative capacitance) mechanism with a response time in the range of $\sim 1 - 100$ s. The inductive current process signals the occurrence of a complex interplay between electronic and ionic charges in relation to the interface energetics, which seems to be highly dependent on the surface processing and contacting procedure.

Macroscopic $CH_3NH_3PbBr_3$ ($MAPbBr_3$) perovskite monocrystals were prepared by an inverse temperature crystallization technique[23] using 1 M solution of $PbBr_2$ and MABr in dimethylformamide (DMF) [Fig. 1(a)]. The solution was heated up in an oil bath at 80 °C for about 1 h to obtain the crystals of about 2–5 mm. Samples show a monocrystal morphology as verified by 2D-XRD images (Fig. S1, supplementary material). Crystals were washed with diethyl ether, placed in the vial with argon gas, and transferred to the glove box with a nitrogen atmosphere. Contacts were deposited at two opposite facets with a non-polar solvent

a)Authors to whom correspondence should be addressed: kovalenko.alx@gmail.com and garciag@uji.es, Tel.: +34 964 387538.

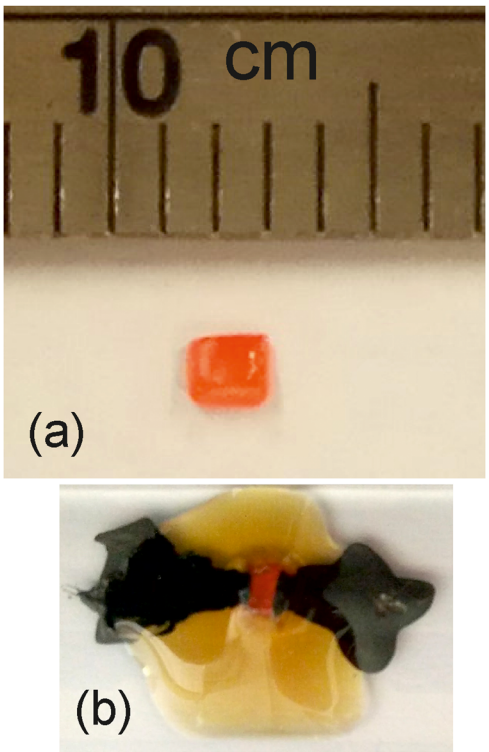

FIG. 1. (a) $CH_3NH_3PbBr_3$ single crystal resulting from the inverse temperature crystallization technique. (b) Perovskite single crystals after carbon paste contacting and epoxy resin encapsulation.

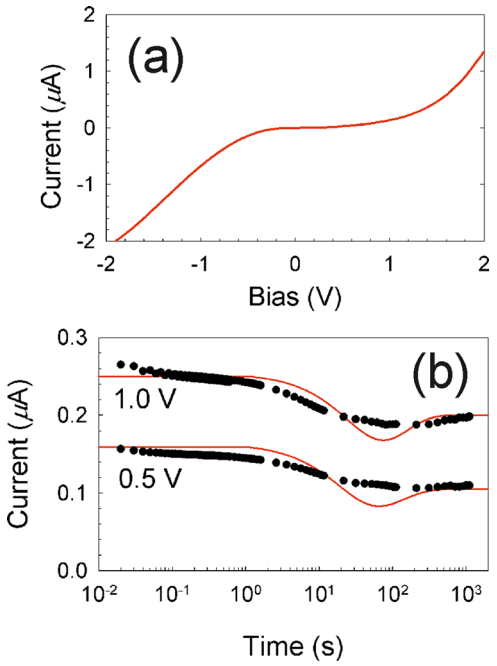

FIG. 2. (a) Example of the reproducible *I-V* curve showing the symmetrical and non-ohmic response. (b) Experimental current transient (dots) using a perovskite single crystal in response to a voltage step from zero to the indicated voltage. The calculated response (solid line) using the proposed equivalent circuit in Fig. 3 is shown. For the simulation, the following set of parameters has been used: $R_0 = 9.5$ MΩ, $R_L = 9.5$ MΩ, $R_C = 4.5$ MΩ, $L = 1000$ MH, and $C = 5$ μF, independently of the voltage step.

(hexane) carbon paste. Then, to avoid the effects of moisture and oxygen, devices were encapsulated with an Ossila epoxy resin and removed from the glove box [Fig. 1(b)]. Transient measurements were performed using Autolab potentiostat at room temperature with no illumination applied for various voltage steps until the current stabilization (∼30 min). Impedance Spectroscopy measurements were performed on a Solartron SI 1260 Impedance/Gain-Phase Analyzer with a Solartron Dielectric Interface 1296 device in ambient conditions, with no illumination applied. The AC voltage was set at 0.05 V, and DC was altered from 0 to 2 V. The following measurements were performed for $3 \times 3 \times 1$ mm^3 crystals.

Figure 2(a) shows a reproducible example of the rather symmetrical *I-V* curve. It is noticeable that the characteristic exhibits non-ohmic responses for positive and negative bias. Figure 2(b) displays an example of the transient response of perovskite single crystals to a voltage step from zero to the voltage indicated in each curve. The measurement is performed for several orders of magnitude by changing the sampling time to avoid data saturation. It is apparent from the transients at short time ($t < 1$ s) that current exhibits a rather constant value. After that point, current decreases and eventually reaches a minimum ($t \approx 100$ s), with a subsequent partial recovering for longer times. Therefore, current undergoes an undershoot that cannot be modeled by using simple *RC* circuit elements. This response requires the incorporation of inductive elements accounting for the current recovering for $t \gg 100$ s. The simplest approach relies upon the phenomenological equivalent circuit drawn in Fig. 3. Each branch accounts for a current contribution that differently evolves with time. The series R_CC subcircuit responses with a current decay and gives rise to the current decrease at intermediate times ($t \approx 1 - 10$ s). The inductive series subcircuit R_LL is responsible for the long-time current increment. The resistive element R_0 provides a constant current contribution. It should be noted that the equivalent circuit in Fig. 3 only accounts for small AC perturbation of a given steady state and long-time (low-frequency) responses. Figure 3 does not convey information about DC equivalents, as those devised for Schottky contacts. The current response of the equivalent circuit in Fig. 3 can be readily derived by calculating the inverse Laplace transform corresponding to the voltage step function $V = V_0u(t)$ as $i(t) = V/Z$, with Z being the impedance of the equivalent circuit. The current transient result as

$$i(t) = V_0\left[\frac{1}{R_0} + \frac{1 - e^{-tR_L/L}}{R_L} + \frac{e^{-t/R_CC}}{R_C}\right], \qquad (1)$$

in which the three contributions are visible. Although more sophisticated equivalent circuits can be devised, transient

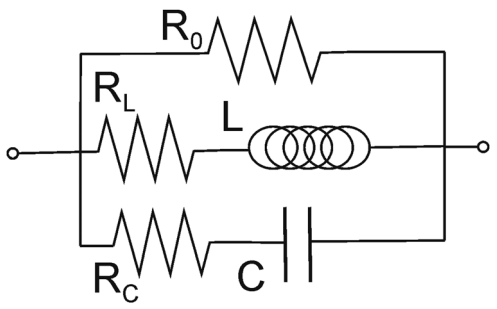

FIG. 3. Equivalent circuit used for transient current simulation showing capacitive and inductive branches.

current is easily simulated to compare it with experimental responses. As observed in Fig. 2(b) (red solid lines), the model in Eq. (1) reproduces the main features, signaling a minimum at intermediate times. The simulation departs from the experimental response because Eq. (1) only includes ideal circuit elements. In addition, the model in Fig. 3 assumes voltage-independent circuit elements. More accurate fitting needs generalized circuit elements (i.e., constant phase elements), with explicit voltage dependences. However, this generalization cannot be readily interpreted and requires additional justifying explanations. This is why modeling is limited to ideal capacitive and inductive elements despite that it provides poorer fitting. In any case, the model in Fig. 3 reproduces the observed current undershoot, which is the central experimental feature. From Eq. (1), one can readily calculate the current limits as $i(0) = V_0[1/R_0 + 1/R_C]$ and $i(\infty) = V_0[1/R_0 + 1/R_L]$.

It is noted that R_0 is necessary to smooth the response near the current minimum that, otherwise, results in excessively abrupt transients. By examining Eq. (1), one can infer the effect of two different time constants related to the RC and RL series coupling as $\tau_C = R_C C$ and $\tau_L = R_L/L$. The experimental data in Fig. 2(b) indicate that $\tau_L > \tau_C$ in order to produce the observed current undershoot, and the simulation provides values as $\tau_C \approx 22$ s and $\tau_L \approx 105$ s. Other parameter combinations as $\tau_L < \tau_C$ or $\tau_L = \tau_C$ do not exhibit any transient minima in Eq. (1). This indicates that the inductive process activates after the capacitor charging. Because of the modeling limitations mentioned above, our approach only captures the essential features of the current response, being the reported characteristic time value estimations of the order of magnitude of the kinetics.

Our experimental conditions, with no light irradiation and symmetrical contacts, are intended to stress carrier injection/extraction over other electronic mechanisms such as carrier recombination. By examining the transient experiments, it is inferred that current is coupled to a capacitive mechanism that is connected in previous works to the ionic polarization at the outer electrodes.[17] The order of magnitude of the capacitor (1–10 μF) signals the formation of an ionic double layer in the vicinity of the perovskite/electrode interface. The initial decrease in current as observed in Fig. 1(c) is then connected to the interface capacitor charging produced by the combined effect of moving ions and injected electrons. The model in Fig. 3 and the fact that $\tau_L > \tau_C$ suggest that electronic carrier extraction is enhanced after capacitor charging. This is electrically represented by the effect of the inductor, provided that the device comprises ion-blocking electrodes, as it is indeed the case because ions are confined within the perovskite material. Iodine vacancies have recently been identified as the prominent mobile defect contributing to electrode polarization.[24] The issue of the influence of the ion distribution within the perovskite bulk and its effect on electronic carrier collection has been recently addressed.[11] In opposition to the effect of extended ion space charge regions entering the absorber bulk, the occurrence of interface ion accumulation layers locates electronic carrier recombination at the outer interfaces and, similarly, makes electronic current highly dependent on the injection/extraction properties of the interfaces.[19]

A related experiment, which allows corroborating the observation of inductive currents by transient methods, is the analysis of low-frequency impedance responses. Although both experiments are not straightforwardly comparable (impedance modulates a steady state, while transients respond to large amplitude voltage steps), inductive fingerprints should indeed occur in impedance responses. From the equivalent circuit in Fig. 3, one can expect that the inductive branch yields a crossing to negative capacitance in the impedance plot ($Z' - Z''$) for lower frequencies. This is what is reported in Fig. 4(a). For 0.5 V DC bias, the impedance develops a large inductive arc, in agreement with the equivalent circuit and the current recovering for long times. Resistances differ from that extracted from transient responses as both techniques are not equivalent. It is noted that for larger voltage polarization [1 V in Fig. 4(a)], the inductive mechanism becomes more featured with multiple negative capacitance arcs. This fact signals the complexity of the interfacial charge extraction mechanism that cannot be modeled by simple equivalent circuits (Fig. 3). For a detailed impedance fitting, see the supplementary material. By examining Fig. 4(b), one can observe how the inductive (negative capacitance) response onset is shifted toward higher frequencies as the voltage increases. This fact implies that the kinetics of inductive currents is fostered by the bias voltage. It is also noted that the time scale of the inductive mechanism kinetics appears to be accelerated when tested with impedance as compared to values exhibited by current transients. Apart from differences in measuring conditions, the variation in surface processing and contacting procedures might be behind the observed dispersion.

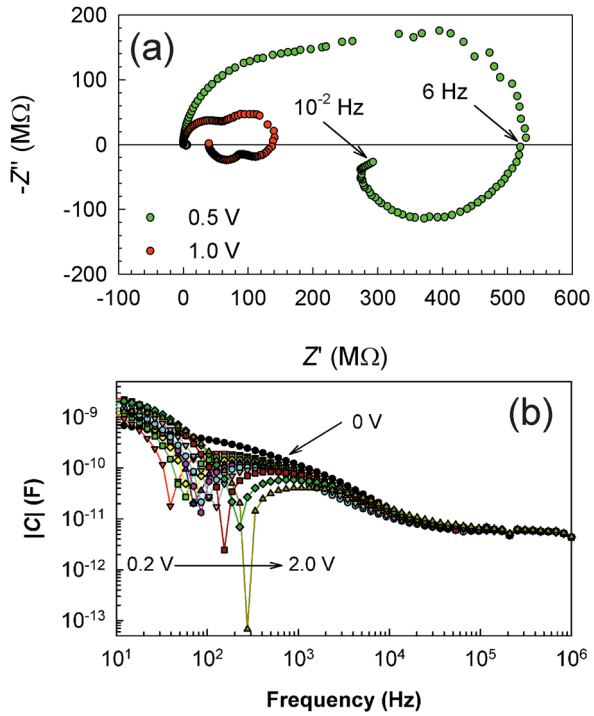

FIG. 4. (a) Impedance plot of perovskite single crystals exhibiting the low-frequency inductive (negative capacitance) response. It is observed that the inductive behavior is more featured for higher potentials. (b) Variation of the capacitance absolute value with bias voltage. At high frequencies, responses collapse to the geometrical capacitance. Singularities point to the quadrant crossing in the onset of the negative capacitance. The 0 V spectrum without induction is marked.

This kind of inductive, low-frequency response has been previously reported for perovskite devices.[25] In some cases, it has been connected to the enhancement of recombination mechanisms[26] or to the interplay between surface polarization and recombination.[20,27] Other works observe inductive loops under vacuum conditions (10^{-3} mbar) and propose electrochemical reactions involving iodine.[28] These explanations are not exclusive. We stress that the observed coupling between capacitive and inductive behavior points to interfaces as the locus governing injection/extraction processes, in agreement with the observation of negative capacitance in electrochemical systems.[29] The fact that accumulation capacitances are measured at low-frequencies[18] locates the current recovering mechanism (induction) also at outer interfaces. As inferred from transient analysis, capacitances exhibit 1–10 μF values, precluding absorbing bulk mechanisms as causing charge accumulation. Models accounting for inductive responses were introduced in the case of single-carrier organic diodes relying upon the dynamic change in occupancy of surface electronic states.[30,31] Those models highlight that carrier extraction depends on the filling/release of interfacial intermediate states which occupation lags with respect to the voltage stimulus. The kinetics of the occupancy may exhibit rather complex behaviors as those observed, at high voltages, in the double inductive response in Figs. 4(a) and S2 (supplementary material). Although much more experimentation is needed here, we can propose that the density and energy distribution of interface states lie behind the featured carrier extraction dynamics. The density and energy position of such interface states may well be influenced by the local distribution of mobile ions so as to expect a coupling between ionic and electronic kinetics. In our measurements, the influence of extrinsic defects can be ruled out as samples are kept in an inert atmosphere during encapsulation.

In summary, our experiments indicate that the electronic carrier injection (both from and into the perovskite material) is a featured mechanism connected to the observation of inductive (negative capacitance) responses. The net effect of these processes is the enhancement in current injection after long term polarization, which is visible both for transient and impedance techniques. It is proposed that the kinetics of surface states is coupled to the migration of ionic charges in such a way that the carrier injection/extraction undergoes intricate dynamics, giving rise to complex current patterns, highly dependent upon surface processing.

See supplementary material for 2D-XRD images, detailed impedance analysis and fitting results.

We thank financial support by Ministerio de Economía y Competitividad (MINECO) of Spain under a project (No. MAT2013-47192-C3-1-R), Generalitat Valenciana (Prometeo/2014/020), and a project GA165S01001 by Czech Science Foundation, Czech Republic. SCIC from UJI is also acknowledged.

[1]J. M. Azpiroz, E. Mosconi, J. Bisquert, and F. De Angelis, Energy Environ. Sci. **8**, 2118 (2015).
[2]T.-Y. Yang, G. Gregori, N. Pellet, M. Grätzel, and J. Maier, Angew. Chem. Int. Ed. **54**, 7905 (2015).
[3]C. Eames, J. M. Frost, P. R. Barnes, B. C. O'Regan, A. Walsh, and M. S. Islam, Nat. Commun. **6**, 7497 (2015).
[4]N. Vicente and G. Garcia-Belmonte, Adv. Energy Mater. **7**, 1700710 (2017).
[5]Z. Li, C. Xiao, Y. Yang, S. Harvey, D. H. Kim, J. A. Christians, M. Yang, P. Schulz, S. U. Nanayakkara, C.-S. Jiang, J. M. Luther, J. Berry, M. C. Beard, M. M. Al-Jassim, and K. Zhu, Energy Environ. Sci. **10**, 1234 (2017).
[6]J. Carrillo, A. Guerrero, S. Rahimnejad, O. Almora, I. Zarazua, E. Mas-Marza, J. Bisquert, and G. Garcia-Belmonte, Adv. Energy Mater. **6**, 1502246 (2016).
[7]S. Cacovich, L. Ciná, F. Matteocci, G. Divitini, P. A. Midgley, A. D. Carlob, and C. Ducati, Nanoscale **9**, 4700 (2017).
[8]K. Domanski, J.-P. Correa-Baena, N. Mine, M. K. Nazeeruddin, A. Abate, M. Saliba, W. Tress, A. Hagfeldt, and M. Grätzel, ACS Nano **10**, 6306–6314 (2016).
[9]C. Li, S. Tscheuschner, F. Paulus, P. E. Hopkinson, J. Kießling, A. Köhler, Y. Vaynzof, and S. Huettner, Adv. Mater. **28**, 2446 (2016).
[10]B. Chen, M. Yang, X. Zheng, C. Wu, W. Li, Y. Yan, J. Bisquert, G. Garcia-Belmonte, K. Zhu, and S. Priya, J. Phys. Chem. Lett. **6**, 4693–4700 (2015).
[11]P. Lopez-Varo, J. A. Jiménez-Tejada, M. García-Rosell, J. A. Anta, S. Ravishankar, A. Bou, and J. Bisquert, ACS Energy Lett. **2**, 1450–1453 (2017).
[12]E. L. Unger, E. T. Hoke, C. D. Bailie, W. H. Nguyen, A. R. Bowring, T. Heumuller, M. G. Christoforo, and M. D. McGehee, Energy Environ. Sci. **7**, 3690 (2014).
[13]W. Tress, N. Marinova, T. Moehl, S. M. Zakeeruddin, M. K. Nazeeruddin, and M. Gratzel, Energy Environ. Sci. **8**, 995 (2015).
[14]G. Garcia-Belmonte and J. Bisquert, ACS Energy Lett. **1**, 683–688 (2016).
[15]S. Meloni, T. Moehl, W. Tress, M. Franckevičius, M. Saliba, Y. H. Lee, P. Gao, M. K. Nazeeruddin, S. M. Zakeeruddin, U. Rothlisberger, and M. Graetzel, Nat. Commun. **7**, 10334 (2016).
[16]O. Almora, I. Zarazua, E. Mas-Marza, I. Mora-Sero, J. Bisquert, and G. Garcia-Belmonte, J. Phys. Chem. Lett. **6**, 1645 (2015).
[17]O. Almora, A. Guerrero, and G. Garcia-Belmonte, Appl. Phys. Lett. **108**, 043903 (2016).
[18]I. Zarazua, J. Bisquert, and G. Garcia-Belmonte, J. Phys. Chem. Lett. **7**, 525–528 (2016).
[19]I. Zarazua, G. Han, P. P. Boix, S. Mhaisalkar, F. Fabregat-Santiago, I. Mora-Seró, J. Bisquert, and G. Garcia-Belmonte, J. Phys. Chem. Lett. **7**, 5105–5113 (2016).
[20]E. Ghahremanirad, A. Bou, S. Olyaee, and J. Bisquert, J. Phys. Chem. Lett. **8**, 1402–1406 (2017).
[21]Y. Liu, Z. Yang, D. Cui, X. Ren, J. Sun, X. Liu, J. Zhang, Q. Wei, H. Fan, F. Yu, X. Zhang, C. Zhao, and S. F. Liu, Adv. Mater. **27**, 5176 (2015).
[22]W. Peng, L. Wang, B. Murali, K.-T. Ho, A. Bera, N. Cho, C.-F. Kang, V. M. Burlakov, J. Pan, L. Sinatra, C. Ma, W. Xu, D. Shi, E. Alarousu, A. Goriely, J.-H. He, O. F. Mohammed, T. Wu, and O. M. Bakr, Adv. Mater. **28**, 3383 (2016).
[23]M. I. Saidaminov, A. L. Abdelhady, B. Murali, E. Alarousu, V. M. Burlakov, W. Peng, I. Dursun, L. Wang, Y. He, G. Maculan, A. Goriely, T. Wu, O. F. Mohammed, and O. M. Bakr, Nat. Commun. **6**, 7586 (2015).
[24]A. Senocrate, I. Moudrakovski, G. Y. Kim, T.-Y. Yang, G. Gregori, M. Grätzel, and J. Maier, Angew. Chem. Int. Ed. **56**, 7755–7759 (2017).
[25]R. S. Sanchez, V. Gonzalez-Pedro, J.-W. Lee, N.-G. Park, Y. S. Kang, I. Mora-Sero, and J. Bisquert, J. Phys. Chem. Lett. **5**, 2357 (2014).
[26]Q. Tai, P. You, H. Sang, Z. Liu, C. Hu, H. L. W. Chan, and F. Yan, Nat. Commun. **7**, 11105 (2016).
[27]A. Guerrero, G. Garcia-Belmonte, I. Mora-Sero, J. Bisquert, Y. S. Kang, T. J. Jacobsson, J.-P. Correa-Baena, and A. Hagfeldt, J. Phys. Chem. C **120**, 8023–8032 (2016).
[28]A. Zohar, N. Kedem, I. Levine, D. Zohar, A. Vilan, D. Ehre, G. Hodes, and D. Cahen, J. Phys. Chem. Lett. **7**, 191–197 (2016).
[29]E. Radvanyi, K. V. Havenbergh, W. Porcher, S. Jouanneau, J.-S. Bridel, S. Put, and S. Franger, Electrochim. Acta **137**, 751 (2014).
[30]J. Bisquert, G. Garcia-Belmonte, Á. Pitarch, and H. J. Bolink, Chem. Lett. **422**, 184 (2006).
[31]G. Garcia-Belmonte, H. J. Bolink, and J. Bisquert, Phys. Rev. B **75**, 085316 (2007).